

# Using machine-learning to construct TOMCAT model and occultation measurement-based stratospheric methane (TCOM-CH<sub>4</sub>) and nitrous oxide (TCOM-N<sub>2</sub>O) profile data sets

Sandip S. Dhomse<sup>1,2</sup> and Martyn P. Chipperfield<sup>1,2</sup>

<sup>1</sup>School of Earth and Environment, University of Leeds, Leeds, UK

<sup>2</sup>National Centre for Earth Observation, University of Leeds, Leeds, UK

**Correspondence:** Sandip Dhomse (s.s.dhomse@leeds.ac.uk)

**Abstract.** Monitoring the atmospheric concentrations of greenhouse gases (GHGs) is crucial to improve our understanding of their climate impact. However, there are no long-term profile data sets of important GHGs that can be used to gain a better insight into the processes controlling their variations in the atmosphere. In this study, we apply corrections to chemical transport model (CTM) output based on profile measurements from two solar occultation instruments: the HALogen Occultation Experiment (HALOE) and the Atmospheric Chemistry Experiment - Fourier Transform Spectrometer (ACE-FTS). The goal is to construct long-term (1991-2021), gap-free stratospheric profile data sets, hereafter referred to as TCOM, for two important GHGs.

To estimate the corrections needed to apply to the CTM profiles, we use the Extreme Gradient Boosting (XGBoost) regression model. For methane (TCOM-CH<sub>4</sub>), we utilize both HALOE and ACE satellite profile measurements from 1992 to 2018 to train the XGBoost model, while profiles from 2019 to 2021 serve as an independent evaluation data set. As there are no nitrous oxide (N<sub>2</sub>O) profile measurements for earlier years, we derive XGBoost-derived correction terms to construct TCOM-N<sub>2</sub>O profiles using only ACE-FTS profiles from the 2004-2018 time period, with profiles from 2019-2021 used for the independent evaluation.

Overall, both TCOM-CH<sub>4</sub> and TCOM-N<sub>2</sub>O profiles exhibit excellent agreement with the available satellite measurement-based data sets. We find that compared to evaluation profiles, biases in TCOM-CH<sub>4</sub> and TCOM-N<sub>2</sub>O are generally less than 10% and 50%, respectively, throughout the stratosphere. The daily zonal mean profile data sets, covering altitude (15–60 km) and pressure (300–0.1 hPa) levels, are publicly available via the following links: <https://doi.org/10.5281/zenodo.7293740> for TCOM-CH<sub>4</sub> (Dhomse, 2022a) and <https://doi.org/10.5281/zenodo.7386001> for TCOM-N<sub>2</sub>O (Dhomse, 2022b).

## 1 Introduction

After carbon dioxide (CO<sub>2</sub>), methane (CH<sub>4</sub>) and nitrous oxide (N<sub>2</sub>O) are currently the two most important anthropogenically emitted greenhouse gases (GHGs) and their concentrations in the atmosphere are increasing at substantial rates (e.g. Meinshausen et al., 2020). Primary natural sources of CH<sub>4</sub> are wetlands, decay of organic waste and livestock whereas anthropogenic sources include landfills and production and transport of coal, natural gas and oil (e.g. Sauniois et al., 2016; Lan et al.,

2021). The primary emission sources for N<sub>2</sub>O are agricultural practices, industrial activities, combustion of fossil fuels and  
25 treatment of solid/liquid waste (e.g. Tian et al., 2020). Importantly, as measured by the global warming potential (GWP), CH<sub>4</sub>  
is about 25 times and N<sub>2</sub>O is about 300 times more potent as GHGs compared to CO<sub>2</sub>.

The lifetime of CH<sub>4</sub> in the troposphere is about 9 years (e.g. Lelieveld et al., 1998), and it is primarily removed through  
oxidation by OH. However, in the stratosphere CH<sub>4</sub> destruction is much slower, hence its local lifetime increases to about  
150 years (Chipperfield et al., 2013). CH<sub>4</sub> oxidation is also an important source of water vapour in the stratosphere which  
30 plays a key role in ozone chemistry via HOx cycles, thereby it also influences the radiative balance in the middle stratosphere.  
The primary atmospheric sink for N<sub>2</sub>O is photolysis (producing N<sub>2</sub> + O) in the stratosphere/mesosphere, therefore it is also a  
long-lived species (lifetime about 120 years (Chipperfield et al., 2013)). A secondary sink for N<sub>2</sub>O is reaction with O(<sup>1</sup>D) to  
produce NO that plays a key role in the middle atmosphere O<sub>3</sub> budget via the NOx cycle. An important aspect is that increases  
in both OH and NO can also have positive impacts on ozone especially in the lower stratosphere, as they help to convert  
35 reactive species to long-lived reservoir species. For example, OH + NO<sub>2</sub> (+ M) leads to HNO<sub>3</sub> formation while CH<sub>4</sub> + Cl leads  
to HCl formation, reducing concentrations of reactive NO<sub>2</sub> and Cl. Additionally, as both CH<sub>4</sub> and N<sub>2</sub>O are long-lived in the  
stratosphere, monitoring their concentrations also help us to understand changes in stratospheric chemistry and dynamics.

However, despite their importance, there are only a few satellite instrument that provide global stratospheric profiles of CH<sub>4</sub>  
or N<sub>2</sub>O. Relatively long-term and high quality data records are available from two solar occultation instruments, the HALogen  
40 Occultation Experiment (HALOE) and the Atmospheric Chemistry Experiment-Fourier Transform Spectrometer (ACE-FTS),  
and limb sounding instruments such as the Michelson Interferometer for Passive Atmospheric Sounding (MIPAS) and the  
Microwave Limb Sounder (MLS). However, each instrument has different spatial and temporal coverage and they use different  
measurement techniques and retrieval algorithms. Hence merging these satellite data to construct a single long-term data set  
for a given species is quite challenging.

Therefore, although stratospheric CH<sub>4</sub> and N<sub>2</sub>O profile data sets were released recently by Hegglin et al. (2021), they did  
45 not attempt to merge data from different satellite instruments. Briefly, these data sets were released as part of the Stratospheric  
and Tropospheric Processes And their Role in Climate (SPARC) Data Initiative, and contain monthly mean zonal mean profiles  
in volume mixing ratio (vmr) units on pressure levels. Data from individual satellite instruments are averaged at 36 latitude  
bins (2.5° latitudinal resolution) and provided on 26 pressure levels ranging from 300 hPa to 0.1 hPa. SPARC CH<sub>4</sub> profile data  
50 is constructed using ACE-FTS (2004–2019), HALOE (1991–2005) and MIPAS (2002–2012) measurements (Hegglin et al.,  
2020). Note that SPARC data uses an earlier (v3.6) version of the ACE-FTS data. For N<sub>2</sub>O there is no data set for the 1990s  
but for later periods SPARC N<sub>2</sub>O data contain monthly mean values from Aura-MLS (based on v4.2), MIPAS (v224), the  
Sub-Millimetre Radiometer (SMR, v2.1), and ACE-FTS measurements. Monthly means values are available only if there are  
more than five valid profiles for a given latitude/altitude range. Monthly mean files are available for individual instruments and  
55 there is no merging or adjustment for different data sets.

To our knowledge, until now no attempt has been made to merge satellite data records to construct long-term stratospheric  
CH<sub>4</sub> and N<sub>2</sub>O profile data sets. Here, we do this by constructing correction terms for the stratospheric CH<sub>4</sub> and N<sub>2</sub>O profiles  
from a chemical transport model by analysing the difference between the model and available satellite observations. Then, the

correction terms (i.e. difference needed to adjust TOMCAT CH<sub>4</sub>/N<sub>2</sub>O profiles) are calculated for all the model grid points to  
60 construct a long-term, gap-free stratospheric profile data set. Details of the satellite data and model set up used here are given in  
Sections 2 and 3, respectively. The methodology used to estimate the correction terms is described in Section 4. Evaluation of  
the newly constructed data sets for CH<sub>4</sub> and N<sub>2</sub>O is presented in Section 5, followed by Summary and Conclusions in Section  
6.

## 2 Satellite data and model setup

65 Being potent GHGs and primary sources of stratospheric water vapour and NO<sub>x</sub>, stratospheric CH<sub>4</sub> and N<sub>2</sub>O measurements  
gained scientific attention even before the discovery of the Antarctic ozone hole (Farman et al., 1985). Initial measurements  
were performed by the Stratospheric and Mesospheric Sounder (SAMS) instruments on Nimbus 7 satellite that was launched  
in 1978 (Drummond et al. (1980); Jones and Pyle (1984)). Similarly, the Atmospheric Trace Molecule Spectroscopy (ATMOS)  
instrument (Gunson et al., 1990) provided about 350 profiles during four space shuttle missions (in 1985, 1992, 1993 and  
70 1994). Later, the Improved Stratospheric and Mesospheric Sounder (ISAMS) was able to provide about 2600 profiles/day for  
about 180 days between 1991-1992, but retrieval was feasible only for the upper stratospheric/mesospheric altitude range (e.g.  
Remedios et al., 1996).

A step-change in the number of stratospheric CH<sub>4</sub> measurements occurred with the deployment of HALOE on the Upper  
Atmosphere Research Satellite (UARS) in September 1991, followed by ACE-FTS in August 2003. Both instruments provided  
75 about 30 profiles per day (discussed below). Two additional instruments, SCIAMACHY (SCanning Imaging Absorption spec-  
troMeter for Atmospheric CHartography) and MIPAS on the Envisat satellite platform also provided useful stratospheric CH<sub>4</sub>  
profiles over the 2003–2012 time period (e.g. Noël et al., 2016, 2018). For N<sub>2</sub>O, the Cryogenic Limb Array Etalon Spectrom-  
eter (CLAES) on the UARS satellite platform provided about one year of profile measurements (October 1991 to July 1992).  
Later, the Sub-Millimetre Radiometer (SMR) on Odin, launched in 2001 (e.g. Urban et al., 2005), MIPAS, and MLS on the  
80 Aura satellite (Waters et al., 2006) also provided very useful N<sub>2</sub>O profile measurements. However, to avoid inter-instrument  
biases likely due to differences in the measurement techniques, we decided here to use only HALOE and ACE-FTS data.

### 2.1 HALOE

HALOE was launched aboard UARS in September 1991 (Russell III et al., 1993). The spacecraft was in a 57° inclined orbit  
at an altitude of ~585 km that allowed for observations from 80°S to 80°N. The HALOE instrument used a combination of  
85 broadband radiometry and gas filter correlation techniques to observe several trace gas species in the spectral range of 2.4–10.4  
μm (or 963–4140 cm<sup>-1</sup>). HALOE provided about 30 measurements (15 sunrise and 15 sunset) per day with near-global  
coverage in approximately one month. In general, daily measurements are provided at two nearly fixed latitudes (sunrise  
and sunset) with near equal longitude spacing. For CH<sub>4</sub> the retrieval algorithm uses a 2855–2915 cm<sup>-1</sup> spectral window  
(channel 6) and profiles are retrieved for the 15 km to 90 km range. The algorithm uses an onion-peeling scheme with 1.5 km  
90 thick tangent layer to calculate the transmission using a forward model thereby achieving about 1.5 km vertical resolution.

Here we use HALOE v19 data that is available for October 1991 to November 2005 time period and is obtained via [https://acdisc.gesdisc.eosdis.nasa.gov/data/UARS\\_HALOE\\_Level2/](https://acdisc.gesdisc.eosdis.nasa.gov/data/UARS_HALOE_Level2/).

## 2.2 ACE-FTS

ACE-FTS was launched aboard the SciSat-1 spacecraft in August 2003 (Bernath, 2002). The spacecraft was launched in a drifting orbit at an inclination of  $74^\circ$  which allows for observations from  $85^\circ\text{S}$  to  $85^\circ\text{N}$ . The ACE-FTS instrument has very high spectral resolution ( $0.02\text{ cm}^{-1}$ ) and covers the spectral range between  $750$  and  $4400\text{ cm}^{-1}$  (Bernath et al., 2005). Similar to HALOE, ACE-FTS uses the solar occultation technique (30 measurements per day). Global latitude coverage is obtained over a period of 3 months and is almost exactly periodic from year to year. The  $\text{CH}_4$  profile retrieval uses about 60 microwindows between  $1244\text{--}3087\text{ cm}^{-1}$  while the  $\text{N}_2\text{O}$  retrieval uses 69 microwindows between  $1120\text{--}2600\text{ cm}^{-1}$  (Strong et al., 2008). Retrieval is performed at  $1\text{ km}$  resolution from about  $5\text{ km}$  to  $70\text{ km}$  (Boone et al., 2020). It is important to note that the ACE retrieval scheme does not use averaging kernels. Rather, it uses a so-called global-analysis-type approach where all data are fitted simultaneously using Levenberg-Marquardt least-squares methods. This means that the vmrs for all the contributing molecules in a given microwindow set are fitted/retrieved simultaneously, which is different to the onion-peeling method adopted for SAGE and HALOE retrievals. Here we use ACE v4.2 data that is obtained via <http://www.ace.uwaterloo.ca/data.php>

## 3 TOMCAT CTM

As both  $\text{CH}_4$  and  $\text{N}_2\text{O}$  are long-lived tracers in the stratosphere, their distributions in this region are largely determined by transport process. Hence, we decided to use profiles simulated by TOMCAT CTM as it is forced with an up-to-date meteorological reanalysis data set. Briefly, TOMCAT is an off-line three-dimensional CTM that includes a comprehensive stratospheric chemistry scheme but, in the version used here, with a simple tropospheric chemical scheme (Chipperfield, 2006). This means concentrations of long-lived ozone depleting substances (ODSs) and GHGs are prescribed as surface mixing ratio boundary conditions (e.g. WMO, 2018) and are assumed to be well mixed throughout the troposphere. For  $\text{CH}_4$  the model uses observed monthly mean global surface concentrations from the National Oceanic and Atmospheric Administration (NOAA) network. The CTM setup is therefore similar to the control simulations used in our recent studies such as Dhomse et al. (2022) and Li et al. (2022). The model simulation is performed at a  $2.8^\circ \times 2.8^\circ$  horizontal resolution with 32 hybrid sigma-pressure levels (surface to about  $60\text{ km}$ ) and is forced with ERA5 (and ERA5.1) reanalysis meteorology (Hersbach et al., 2020). The effects of time-varying solar flux changes and volcanically enhanced stratospheric aerosol are included by using separate time-varying forcing files (e.g. Dhomse et al., 2015, 2016).



## 4 Methodology

120 For stratospheric ozone various methodologies have been adopted to merge different types of data to construct homogenised data sets. They include both simple and complex methodologies for adjusting biases for overlapping time periods (e.g. Hassler et al., 2008, 2018; Arosio et al., 2018), use of multivariate linear models (e.g. Randel and Wu, 2007) and data assimilation (Inness et al., 2015). However, we are not aware of any attempt to construct long-term stratospheric CH<sub>4</sub> and N<sub>2</sub>O profile data sets using different satellite data sets.

125 Here, our approach is similar to that of Dhomse et al. (2021) for ozone who used CTM profiles as a transfer function and estimated model-observation biases using machine learning. However, they used observation-based monthly mean zonal mean ozone values from Stratospheric Water and OzOne Satellite Homogenized (SWOOSH) data set (Davis et al., 2016) rather than individual satellite data products. As there are a number of satellite instruments that provide ozone profile measurements, monthly mean zonal mean values in merged ozone data sets are considered to be well constrained. However, as noted in  
130 Section 2, there are very few satellite instruments that provide CH<sub>4</sub> profile measurements (largely two occultation instruments providing 30 profiles per day), so in this study we decided to use individual data points to train a machine learning algorithm. Similarly, for N<sub>2</sub>O (among occultation instruments) only ACE-FTS provides a long profile data record, but again it has limited spatial coverage hence calculation of monthly mean zonal mean profiles are subject to sampling errors.

Overall, there are 6 steps in our approach. First, TOMCAT output fields are sampled for HALOE and ACE measurement  
135 collocations. There are about 95,000 HALOE profiles and over 106,000 ACE profiles in the 1991-2021 time period. Second, as ACE profiles are available at 1 km vertical resolution, HALOE profiles are also binned at 1 km vertical resolution and TOMCAT profiles (surface to 60 km) are interpolated to the same grid.

Third, we calculate observation-TOMCAT profile differences for each 1 km grid and satellite measurements are included only if retrieval errors are less than 100% and retrieved values are greater than zero. Note that we assume that all the measure-  
140 ments with retrieval errors less than 100% are more or less the absolute truth. Hence, no other uncertainties are considered in the further calculations. Our attempt is to construct profile data that would approximate HALOE/ACE data if the instruments had denser measurements without any temporal gaps. As there are distinct dynamical (and chemical) regimes in the stratosphere in terms of processes controlling the distribution of these two GHGs, we divide global measurements into five latitude bins: southern hemisphere (SH) polar (SHpol, 50°S-90°S), SH mid-latitude (SHmid, 20°S-70°S), tropical (40°S-40°N), northern  
145 hemisphere (NH) mid-latitude (NHmid, 20°N-70°N) and NH polar (NHpol, 50°N-90°N). A 20° (10° from either side) latitudinal overlap between the bins is allowed to include possible extreme variations in the training data set. Estimated differences for overlapping grids are averaged in order to avoid possible sharp edges near the latitude bin boundaries.

Fourth, we train the XGBoost regression model for TOMCAT-observation differences of CH<sub>4</sub> or N<sub>2</sub>O for each vertical level. This means there is a separate model for each vertical level (46 for 15-60 km) for each of the 5 latitudinal bins. Briefly,  
150 XGBoost is a supervised machine learning algorithm that uses an ensemble of decision trees (e.g. Chen and Guestrin, 2016). XGBoost applies the principle of boosting weak learners using the gradient descent architecture (Gradient Boosting) with some additional components such as L1 and L2 (Lasso and Ridge) regularization that helps to prevent over-fitting. There

are 13 explanatory variables (or features) in our XGBoost regression model taken from TOMCAT output fields or the ERA5 reanalyses used to force the model. For example, the XGBoost regression model for  $CH_4$  can be represented as:

155

$$dCH_4 = \beta_1 CH_4 + \beta_2 O_3 + \beta_3 N_2O + \beta_4 HNO_3 + \beta_5 HCl + \beta_6 H_2O + \beta_7 HF + \beta_8 NO_2 + \beta_9 ClONO_2 + \beta_{10} T + \beta_{11} PV + \beta_{12} \Theta + \beta_{13} t + \epsilon \quad (1)$$

where  $T$  and  $PV$  are temperature and potential vorticity from ERA5 at co-located TOMCAT grid points. Measurement latitude ( $\Theta$ ) and date ( $t$ ) variables are included to represent temporal/spatial variations in the measurements, whereas  $\epsilon$  denotes unexplained errors. Variables  $\beta_1$  to  $\beta_{13}$  can be considered as the contribution coefficient for a given explanatory variable. For  $CH_4$ , we include an additional (14<sup>th</sup>) step-function-like term in the XGBoost model that is set to 0 for the HALOE time period and 1 for the ACE-FTS time period. Our approach here is to assume that nearly all differences in the TOMCAT  $CH_4$  or  $N_2O$  profiles with respect to HALOE and ACE data arise from the incorrect representation of the chemical and dynamical processes in the CTM (including inhomogeneities in ERA5 data that are used to drive TOMCAT transport). Our aim is to find correction terms for the TOMCAT  $CH_4$  or  $N_2O$  profiles so that they match observational profiles for a particular distribution of model tracers and dynamical set up. Hence, we include nine tracers of varied lifetimes (i.e.  $CH_4$ ,  $O_3$ ,  $N_2O$ ,  $HNO_3$ ,  $HCl$ ,  $H_2O$ ,  $HF$ ,  $N_2O$ ,  $ClONO_2$ ) from TOMCAT. We are aware that some tracers are correlated as all the variables are from a TOMCAT simulation (or forcing meteorology), hence we use Lasso (L1) regularisation option to remove less important variables in case one or some of them are highly correlated at a particular level. We use Python package XGBoost ([https://xgboost.readthedocs.io/en/stable/python/python\\_intro.html](https://xgboost.readthedocs.io/en/stable/python/python_intro.html)) for the analysis with following options:  $n\_estimators=1000$ ,  $max\_depth=4$ ,  $alpha=0.3$ ,  $learning\_rate=0.1$ ,  $min\_child\_weight=6$ . As mentioned earlier, profiles prior to 2018 are used for training (70%) and testing (30%) XGBoost for individual vertical levels. As an additional check, we use the last three years (2019–2021) of data points for the evaluation.

Fifth, we sample daily TOMCAT output at 1:30 and 13:30 UTC equatorial crossing times (day and night time sampling). TOMCAT 3D fields are then re-gridded at 1 km vertical resolution before dividing them into five latitude bins (see above). Trained XGBoost regression models are then used to calculate correction terms for all twice-daily 3D output profiles.

Sixth, correction terms for individual model grid points are merged to construct twice daily (1:30 and 13:30 UTC) 3D (longitude/latitude/height) correction terms. As mentioned above, we use simple averaging for the overlapping grid points to avoid sharp boundaries, followed by simple 2-dimensional (latitude-longitude) smoothing using 3-point boxcar smoothing. These twice daily correction terms are then added to the original TOMCAT  $CH_4$  and  $N_2O$  profiles. Daily mean 3D (longitude/latitude/height) correction terms are calculated by averaging 1:30 and 13:30 UTC fields, followed by zonal means (latitude/height) to produce daily mean zonal mean TCOM- $CH_4$  and TCOM- $N_2O$  profiles.

## 5 Results

As noted in the Introduction,  $CH_4$  and  $N_2O$  concentrations in the lower stratosphere are largely controlled by dynamical processes. The reanalysis data sets used to drive transport in the CTM can be considered as our best knowledge of the past

185

atmosphere as they attempt to incorporate most of the available high quality meteorological observations using data assimilation. However, they are prone to issues related to changes in the number and type of observations assimilated in the reanalysis system, which might introduce inhomogeneities in the data sets produced. On the other hand, although chemical models are ideal tools for simulating and understanding past changes in these two greenhouse gases using consistent chemical schemes, they are also prone to deficiencies. For example, some computationally expensive processes (e.g. vertical mixing in the troposphere) are represented by somewhat simplified parameterisations. Additionally, most of the chemical reaction rates (loss rates) calculated in the model scheme can also have large uncertainties. Hence, chemical-transport-model-simulated profiles often show some kind of bias with respect to observational data sets. Similarly, although occultation-technique-based instruments measure atmospheric spectra at relatively high resolution, they also include simplified parameterisations for complex radiative processes (e.g. scattering, contribution from interfering gases) and so retrieval errors are also sensitive to changes in stratospheric conditions. Hence, here we assume that some of the differences between TOMCAT and observations could be attributed to the distribution of other TOMCAT tracers. We use XGBoost to identify possible interconnection patterns between TOMCAT CH<sub>4</sub> or N<sub>2</sub>O differences and other tracers using available data points so that corrections can be estimated for all model grid points.

Figure 1 shows vertical profiles of estimated variance ( $R^2$ ) and feature (explanatory variable) importances for the SHpol (50°S-90°S) latitude bin for the XGBoost regression model. Feature importance can be considered as a regression coefficient indicating how much a given variable contributes towards the CH<sub>4</sub> or N<sub>2</sub>O bias-correction prediction. Variance and feature importances for SHmid, tropics, NHmid and NHpol are shown in Supplementary Figures S1 to S4, respectively. For SHpol, XGBoost seems to show excellent performance for both species throughout the stratosphere with  $R^2$  values ranging from 0.6 to 0.8. This also validates our approach of using different long-lived tracers as variables in the regression model. As expected, concentrations of long-lived tracers seem to show close relationships to the biases seen in CH<sub>4</sub> and N<sub>2</sub>O profiles. However, supplementary Figures S1 to S4 show that  $R^2$  for other latitude bins are somewhat smaller (near 0.5) indicating regions with less dynamical variability (e.g. mid-latitudes) might need some additional features that are not included in this set up.

Another important aspect is that  $R^2$  values for CH<sub>4</sub> remain almost flat between 25 to 50 km, but for N<sub>2</sub>O,  $R^2$  values are close to 0.6 in the lower stratosphere and lower mesosphere with minima near 30 km. The time (date) term is included in the XGBoost model to allow it to extrapolate corrections to data that lie outside the training period. However, in current setup, the feature importance of the time term is only significant at a few levels for some latitude bands (Figure 1 and Supplementary Figures S1 to S4). This suggests that the time term is not playing a major role in the model's predictions for these latitude bands. To improve the model's performance, we also tried to increase the number of trees, using Huber/quantile loss functions, but none of the changes helped to improve the significance of the time term. In summary, in the current setup the time (date) term is not very important.

In Figure 1, dynamical variables such as potential vorticity are most important in explaining the biases in the lower stratosphere (near 18 km). This is likely due to the fact that the TOMCAT model in the setup employed here overestimates the fast isentropic transport in the lower stratosphere. However, it is important to note that the 50°S-90°S region covers a large part of the high-latitude stratosphere and includes the strong wintertime polar vortex as well as tracer variations near the edge of the

vortex. As a result, it is not possible to attribute the biases to a single variable or process. For example, temperature variations explain a large part of the CH<sub>4</sub> biases around 35 to 40 km, but ClONO<sub>2</sub> is most important just below 35 km. On the other hand, HNO<sub>3</sub> is most important for explaining the N<sub>2</sub>O biases in the mid-upper stratosphere. This suggests that, while there is a strong relationship between temperature, potential vorticity, and chlorine activation, the biases in CH<sub>4</sub> and N<sub>2</sub>O at a single  
225 level are generally better explained by a single variable.

For CH<sub>4</sub>, additional features showing significant importances are water vapour, CH<sub>4</sub> and N<sub>2</sub>O. As CH<sub>4</sub> is the largest in-situ source of stratospheric water vapour, their alternating importances in the lower mesosphere (above 55 km) indicate issues with HOx-related CH<sub>4</sub> loss in the lower mesosphere. On the other hand, in the lower stratosphere, a strong winter-time dehydration inside the polar vortex leads to substantial drying. Hence, the somewhat larger importance for water vapour near 15 km and  
230 23 km suggests that XGBoost is able to identify and attribute possible biases in TOMCAT setup to downward transport of CH<sub>4</sub> as well as the parameterised dehydration scheme. Similarly, the peaks in N<sub>2</sub>O importance near the stratopause (~48km) and near 21 km indicate issues in the representation of the downward transport of the long-lived tracers from the mesosphere into the stratosphere in the polar vortex. Note that in our simulations the TOMCAT top model level is located near 60 km.

Next we compare vertical CH<sub>4</sub> profiles from TOMCAT, TCOM-CH<sub>4</sub> and collocated HALOE/ACE for the SHpol latitude  
235 bin (Figure 2). Overall, we have about 40,000 profiles of which around 30,000 fall in the XGBoost training period and about 10,000 profiles in the 2019-2021 evaluation period. Overall, TCOM-CH<sub>4</sub> profiles show excellent agreement with satellite profiles and median lines seems to follow each other very closely. In contrast the TOMCAT profiles show good agreement with observational data between 20-30 km but exhibit positive biases at upper and lower levels. This distinct feature indicates a clear separation in the importance of dynamical and chemical processes controlling CH<sub>4</sub> concentrations. As mentioned  
240 earlier, positive biases in TOMCAT CH<sub>4</sub> in the lower stratosphere could be due to faster CH<sub>4</sub> transport from the tropics to high-latitudes. Positive biases in the upper stratosphere/lower mesosphere are most probably due to slower CH<sub>4</sub> loss via HOx and ClOx chemistry. Another important characteristic in Figure 2 is that variability in observational profiles (shaded region shows 10 and 90 percentiles) is much larger than TOMCAT (or TCOM) profiles. A possible explanation for differences in variability would be model output is sampled at the longitude/latitude recorded at 30 km tangent height, but in reality collocations  
245 at different altitudes are a few degrees apart. Additionally, the onion-peeling algorithm used for some solar occultation measurements (such as SAGE, HALOE) assumes observations at different tangent height are independent, hence retrieved profiles show larger fluctuations.

Vertical profiles of the absolute (in ppm) and percentage (%) CH<sub>4</sub> differences between the three data sets are also shown in Figure 2 for both the training (1992-2018) and evaluation (2019-2021) time periods. As expected, the median TCOM-CH<sub>4</sub>  
250 profiles show very little difference with respect to collocated median satellite profiles whereas the TOMCAT profile differences range from -0.22 ppm (16 km) to -0.05 (near 28 km). In terms of relative differences, again TCOM-observation differences are close to 0%, whereas for the evaluation period differences are up to 10% in the lower and middle stratosphere. A possible explanation for somewhat larger differences for 2019-2021 time period is that there has been rapid increase in atmospheric CH<sub>4</sub> over last few years (e.g. Nisbet et al., 2019). As the rapid CH<sub>4</sub> increase period is outside XGBoost training values, the  
255 estimated correction terms seem to be too small, but there are still significant improvements compared to TOMCAT profiles.

Median profile comparisons for training and evaluation periods, and subsequent differences (in ppm and %) for other latitude bins, are shown in Supplementary Figures S5 to S8. Again, the TCOM-observation comparison is also consistent for other latitude bins, with an exception that mid-stratospheric biases for evaluation period are somewhat larger (up to 10%) for SH mid-lat and tropics (Figures S5 and S6).

260 Similarly for N<sub>2</sub>O, Figure 3 compares median profiles from ACE-FTS N<sub>2</sub>O, TCOM-N<sub>2</sub>O and TOMCAT and their differences (absolute and percentage) for SH polar latitudes. Again, TCOM-N<sub>2</sub>O and ACE-FTS profiles show excellent agreement for all stratospheric altitudes. Interestingly, TOMCAT N<sub>2</sub>O profiles are high-biased only in the lower stratosphere (up to 25 km) and have negligible biases in the mid-upper stratosphere. So, in the lower stratosphere TOMCAT profiles show positive biases of up to ±50 ppb, while TCOM-N<sub>2</sub>O biases are close to zero for the training period (2004–2010) but show a slight increase  
265 (up to ±10 ppb) for the evaluation period (2019–2021). Some of these biases could be linked to the use of measurements with positive values only, as well as missing a possible variable that would account for strong seasonal variations at higher latitudes in the current set up for XGBoost. Although TCOM-N<sub>2</sub>O biases are much smaller throughout the stratosphere, in percentage terms they can reach up to 100% near 40 km as changes in the small values can translate into much larger changes in relative differences. However, even with those large relative differences, significantly reduced biases in TCOM-N<sub>2</sub>O profiles are visible  
270 for all the levels.

Median profile comparisons and differences between ACE-FTS, TCOM-N<sub>2</sub>O, TOMCAT profiles (in ppb and %) for other latitude bins are shown in Supplementary Figures S9 to S12. Similar to SHpol, the absolute median differences between observed and TCOM values for other latitude bins are less than 10 ppb. However, the relative differences in the upper stratosphere are much larger (up to 100%, especially in the SH midlat and tropics). This is likely due to the fact that TCOM only uses only  
275 positive values, which removes observed profiles with low concentration values during the winter months.

Improvements in CH<sub>4</sub> and N<sub>2</sub>O profiles are clearly visible in time series comparisons shown in Figures 4 and 5 which compare CH<sub>4</sub> and N<sub>2</sub>O evaluations at 20, 30, 40 and 50 km for the SHpol latitude bin. For clarity the figure shows every 10th profile (10% of data points). Similar comparisons for SHmid, tropics, NHmid and NHpol are shown in Supplementary Figures S13 to S20. TCOM-CH<sub>4</sub> data points show excellent agreement with the HALOE and ACE data points (Figure 4). Uneven  
280 data density before and after 2004 reflect differences in viewing techniques between these two satellite instruments. Basically, HALOE was designed to provide near-global coverage whereas ACE-FTS was designed to provide denser coverage at high latitudes. Even with these uneven sampling frequencies, we do not observe any abrupt changes in TCOM-CH<sub>4</sub> data points.

Similarly for N<sub>2</sub>O, Figure 5 also shows excellent agreement between TCOM-N<sub>2</sub>O and ACE-FTS data points. Again the largest corrections are observed in the lower stratosphere (15 to 25 km) where TOMCAT profiles are about 30 ppb high-biased  
285 which can be considered as a systematic bias due to the TOMCAT setup. Similar to CH<sub>4</sub>, a seasonal minimum occurs just after the break-up of Antarctic polar vortex (October) as the descending branch of stratospheric circulation transports N<sub>2</sub>O-depleted air to lower altitudes and latitudes (horizontal mixing). As N<sub>2</sub>O mixing ratios decrease rapidly with increasing altitude, a large number of ACE-FTS data points show negligible N<sub>2</sub>O values which is reflected in TCOM-N<sub>2</sub>O data points. However, it is also important to note that both CH<sub>4</sub> and N<sub>2</sub>O mixing ratios decrease rapidly with increasing altitude (especially during  
290 SH autumn/winter). As the forward model used in the ACE-FTS retrieval algorithm needs spectra on a fixed height levels, a

seasonal variation in vertical structure of the atmosphere alters the spacing between tangent heights. Therefore, N<sub>2</sub>O (as well as CH<sub>4</sub>) profile variability increases when tangent heights get very close together. Additionally, as mixing ratio values get close to zero, retrieved profiles become noisy as some values can be negative. Here, we use only positive data points for XGBoost training, so the correction terms used here might be positively biased, influencing the seasonal cycle effects in CH<sub>4</sub> and N<sub>2</sub>O concentrations.

An important aspect seen in Figures 4 and 5 is that the seasonal cycles in TCOM-CH<sub>4</sub> and TCOM-N<sub>2</sub>O data points seem to be more synchronised with observational data sets than TOMCAT, especially at 20 km. As shown above, TOMCAT profiles show positive biases throughout the stratosphere and the largest corrections seem to be in the summertime maximum values that must arise from transport from mid-high latitudes. Interestingly, near 30 km points from all three data sets seem to be closer to each other for both CH<sub>4</sub> and N<sub>2</sub>O. Finally, an interesting aspect in both Figures 4 and 5 is that in the upper stratosphere both species show wintertime minima near 40 to 50 km that are close to zero throughout the data record. Even with long-term trends in tropospheric concentrations, a casual inspection does not show any significant trends in either species. We aim to explore this aspect of CH<sub>4</sub> and N<sub>2</sub>O trends in future studies.

Next we compare TCOM-CH<sub>4</sub> profiles with the latest SPARC CH<sub>4</sub> data set (Hegglin et al., 2021). Figure 6 show daily mean zonal mean CH<sub>4</sub> time series from TCOM-CH<sub>4</sub> and monthly mean values from three SPARC (S-HALOE-CH<sub>4</sub>, S-MIPAS-CH<sub>4</sub> and S-ACE-CH<sub>4</sub>) CH<sub>4</sub> data records. Unsurprisingly, with some exceptions (near 32.5°S and N), TCOM-CH<sub>4</sub> shows best agreement with S-ACE-CH<sub>4</sub> data at all pressure levels and latitude bins. At 50 hPa, TCOM-CH<sub>4</sub> values show somewhat positive biases with respect to S-HALOE-CH<sub>4</sub> near subtropical latitudes, but relatively better agreement in the middle (5 hPa) and upper (0.5 hPa) stratosphere. On the other hand, S-MIPAS-CH<sub>4</sub> data points show significant positive biases with respect to all other data records with qualitative agreement in the upper stratosphere. Additionally, as expected, positive growth rates observed in the tropospheric CH<sub>4</sub> concentrations are also distinguishable in both observations (ACE + HALOE) and TCOM-CH<sub>4</sub> data especially near tropical and subtropical latitudes at 50 hPa.

Figure 6 also compares the CH<sub>4</sub> evolution at 67.5° S and 67.5° N. As expected, wintertime CH<sub>4</sub> concentrations in the SH high latitudes are somewhat larger compared to the NH high-latitudes (e.g. Remsberg, 2015). This is because a stronger Brewer-Dobson (BD) circulation in the NH causes faster downward propagation of the CH<sub>4</sub>-poor air from the upper stratosphere to the lower-middle stratosphere. Interestingly, all the SPARC CH<sub>4</sub> data records show less CH<sub>4</sub> in the SH at 50 hPa than TCOM. At 5 hPa, TCOM-CH<sub>4</sub> data show relatively better agreement with S-HALOE-CH<sub>4</sub> data in both hemispheres and with S-ACE-CH<sub>4</sub> data only in the NH. The exact causes of unusually low CH<sub>4</sub> values in S-MIPAS-CH<sub>4</sub> and S-ACE-CH<sub>4</sub> data files are unclear. A possible explanation might be absence of negative data points seen in ACE data (due to enhanced winter-time downwards transport of CH<sub>4</sub>-poor air) are excluded in the XGBoost training step. It also suggests that winter-time downward descent at higher latitudes is somewhat weaker in TCOM data. Again, S-MIPAS-CH<sub>4</sub> data points indicate a much larger magnitude of seasonal cycle compared to other data sets. In the upper stratosphere (0.5 hPa), there seems to be better agreement among all the data in both hemispheres. Overall, we find that compared to the TCOM-CH<sub>4</sub> data set, SPARC CH<sub>4</sub> data records have some inconsistent characteristics and the largest disagreement is found to be at NH high latitudes.

325 Figure 7 compares the evolution of TCOM-N<sub>2</sub>O and SPARC data sets based on MIPAS, Aura-MLS, SMR and ACE measurements for five latitude grids (67.5°S, 32.5°S, 2.5°N, 32.5°N, and 67.5°N) and three pressure levels (50 hPa, 5 hPa, and 0.5 hPa). The lack of satellite measurements during the 1990s makes it difficult to compare the long-term N<sub>2</sub>O evolution but significant differences between various satellite data records also complicate the more straightforward evaluation. Overall, TCOM-N<sub>2</sub>O shows best agreement with SPARC ACE-FTS (S-ACE-N<sub>2</sub>O) data and poorest agreement with SPARC MIPAS  
330 (S-MIPAS-N<sub>2</sub>O) data. Interestingly, SPARC SMR (S-SMR-N<sub>2</sub>O) show N<sub>2</sub>O variations that are very similar to the S-MIPAS-N<sub>2</sub>O data set whereas SPARC-Aura-MLS (S-AMLS-N<sub>2</sub>O) agrees better with S-ACE-N<sub>2</sub>O, with some exceptions in the later few years that are related to a drift in MLS N<sub>2</sub>O measurement (190 GHz) channel (Livesey et al., 2021), especially in the lower stratosphere. Hence, for the earlier period TCOM-N<sub>2</sub>O also shows good agreement with S-AMLS-N<sub>2</sub>O data until 2014 and then slight drifts are distinguishable at low-mid latitudes. On the other hand, the close agreement between S-SMR-N<sub>2</sub>O  
335 and S-MIPAS-N<sub>2</sub>O means that both data sets exhibit high biases in the lower stratosphere and again agreement is weakest at low-mid latitudes.

Another important aspect in Figure 7 is that at high latitudes, as well as for mid-upper stratospheric altitudes, all the SPARC data sets agree quite well with each other and there are no long-term drift and systematic biases between them. The good agreement of TCOM-N<sub>2</sub>O with all the SPARC N<sub>2</sub>O data sets at 5 and 0.5 hPa provides additional evidence of the usefulness of  
340 the TCOM-N<sub>2</sub>O data set. Additionally, similar to TCOM-CH<sub>4</sub>, casual inspection of TCOM-N<sub>2</sub>O does not show any long-term trends at mid-upper stratospheric pressure levels; we aim to investigate this further in future studies.

Next we analyse differences between TCOM-CH<sub>4</sub> and TOMCAT CH<sub>4</sub> profiles through the time evolution of corrections estimated by the XGBoost regression model. First we look at the differences in zonal mean CH<sub>4</sub> at different levels. Figure 8 shows TCOM-CH<sub>4</sub> minus TOMCAT CH<sub>4</sub> differences (in %) at four vertical levels (15 to 45 km with 10 km spacing).  
345 An important aspect regarding 15 km and 25 km differences is that although median CH<sub>4</sub> differences shown in Figure 2 indicate TOMCAT profiles show positive biases (up to 10%), the latitude slice indicates significant variations between the two. Differences are even positive close to polar latitudes indicating stronger downward transport of CH<sub>4</sub>-poor air and/or weaker mixing near the Antarctic polar vortex region in the TOMCAT simulation. Similar characteristics are observed at NH high latitudes. These biases are even more distinct at 25 km, especially in the SH high latitudes, though this region can be  
350 considered to be a boundary region where dynamical processes control CH<sub>4</sub> concentrations at lower altitudes and chemical processes dominate at higher altitudes. Inter-hemispheric asymmetry in the CH<sub>4</sub> bias correction also indicates significant differences in the representation of the BD circulation in ERA5 data (e.g. Li et al., 2022).

Additionally, some uneven differences for 1991-1993 at 15 and 25 km in Figure 8 could be due to a combination of various chemical and dynamical processes. For example, volcanically enhanced stratospheric aerosol following the Mt. Pinatubo eruption in June 1991, might have altered stratospheric transport pathways as larger aerosols absorb outgoing long-wave radiation  
355 (Free and Lanzante, 2009; Dhomse et al., 2020). Such heating can also enhance tropical upwelling as well as horizontal mixing on isentropic surfaces (e.g. Poberaj et al., 2011; Dhomse et al., 2015; Bittner et al., 2016). Volcanically enhanced stratospheric aerosol can also alter OH radical concentrations either by modulating the amount of incoming solar radiation or by altering chemical pathways (e.g. Bândă et al., 2013, 2016). It is also well known that increases in stratospheric aerosol concentration

360 also affected HALOE retrievals (e.g. Remsberg, 2008). ERA5 data assimilation does not include these atmospheric effects of volcanically enhanced stratospheric aerosol (e.g. Hersbach et al., 2020), hence we are not sure about the unusual CH<sub>4</sub> differences in the lower stratosphere.

On the other hand, differences at 35 km in Figure 8 seem to be dominated by the QBO-induced meridional circulation patterns (e.g., Baldwin et al., 2001), that are underestimated in TOMCAT. Even though ACE provides limited observational  
365 data points in the tropics, XGBoost is able to identify this discrepancy. On the temporal scale, differences are largest until 1996, reaching polar latitudes, followed by gradual decrease in the NH sub-tropics and remain larger in the SH sub-tropics. A similar type of uneven evolution for later periods can also be seen, suggesting issues in ERA5 data towards the representation of QBO-induced circulation, especially for years with an unusual QBO evolution such as 2016 and 2020 (e.g. Newman et al., 2016; Osprey et al., 2016; Diallo et al., 2022).

370 Another notable feature in Figure 8 is that at 45 km, for some years, CH<sub>4</sub> differences are clearly distinguishable. Both HALOE and ACE have much smaller retrieval errors at higher altitudes and, assuming there were no abrupt changes in these two satellite instruments (or retrieval algorithms), the unusual differences seen at 45 km can be attributed to inhomogeneities or issues in ERA5 data. These distinctive periods include the first halves of years 1993, 1997, 2001, 2004 and the latter half of 2019.

## 375 **6 Summary and Conclusions**

Even though CH<sub>4</sub> and N<sub>2</sub>O are very important greenhouse gases, as well as the sources for key stratospheric species, there are limited stratospheric profile data sets that extend for more than a decade. Due to their long lifetimes, CH<sub>4</sub> and N<sub>2</sub>O are also very useful dynamical tracers that can be used to evaluate stratospheric transport processes. Also, accurate stratospheric CH<sub>4</sub> profiles are a valuable constraint for the retrieval of tropospheric methane using satellite instruments. However, until now no  
380 attempt has been made to construct long-term CH<sub>4</sub> and N<sub>2</sub>O profile data sets. Furthermore, although chemical models are able to simulate long-term profile data sets of these species, they are highly dependent on the representation of individual chemical and dynamical processes in a particular model.

Here we have used CH<sub>4</sub> and N<sub>2</sub>O profiles from the TOMCAT CTM, two solar occultation instrument measurements and the eXtreme Gradient Boost (XGBoost) regression model to construct daily, gap-free stratospheric profile data sets (TCOM-CH<sub>4</sub>  
385 and TCOM-N<sub>2</sub>O) for the 1991-2021 time period. The XGBoost regression model is trained for the CH<sub>4</sub> or N<sub>2</sub>O difference between TOMCAT and satellite measurements (HALOE and ACE). These differences are used to estimate corrections that are added to the TOMCAT profiles to derive TCOM-CH<sub>4</sub> and TCOM-N<sub>2</sub>O profiles. The regression algorithm uses 13 features (or variables) based on TOMCAT tracers as well as four additional features such as temperature, potential vorticity, latitude and date of the measurement. Because atmospheric concentrations of CH<sub>4</sub> and N<sub>2</sub>O vary due to distinct dynamical and chemical  
390 processes in different regions, our approach involves dividing global measurements into five latitude-based categories. These categories include two for the polar regions, two for mid-latitudes, and one for the tropics. We then proceed to derive regression parameters for each 1 km vertical grid spanning from 15 to 60 km within each of these latitude bins.



For both gases considered, XGBoost shows good performance ( $R^2 > 0.5$  to 0.8) throughout the stratosphere, except for lower stratosphere which can be attributed to the limited training measurements. Measurements from the final three years (2019-2021) are used to evaluate TCOM-CH<sub>4</sub> and TCOM-N<sub>2</sub>O profiles. Overall, TCOM-CH<sub>4</sub> shows excellent agreement with the evaluation profiles and median differences are less than 10%. Additionally, comparison with SPARC-CH<sub>4</sub> data suggests that SPARC-MIPAS profiles show some unrealistic behaviour and SPARC-ACE and SPARC-HALOE do not show expected inter-hemispheric differences in lower stratospheric CH<sub>4</sub> differences (less CH<sub>4</sub> in the NH).

For TCOM-N<sub>2</sub>O, better agreement is again seen with respect to S-ACE-N<sub>2</sub>O data set and weaker agreement is observed against MIPAS data. TCOM-N<sub>2</sub>O also confirms the abnormal drift in Aura-MLS v4.2 N<sub>2</sub>O data (as used in SPARC data set) especially at lower latitudes and altitudes (e.g. Livesey et al., 2021). A casual inspection of TCOM-CH<sub>4</sub> and TCOM-N<sub>2</sub>O plots also suggests that despite increasing surface values there are near-negligible long-term trends in the upper stratosphere/lower mesosphere which is consistent with Minganti et al. (2022). On the other hand, (Prather et al., 2022) analysed MLS V5 data to show positive trends (up to 15%) in the tropical upper stratospheric N<sub>2</sub>O, though they do not find NO production rising at the similar rates. A possible explanation would be stratospheric/mesospheric loss processes probably determined by changes in the stratospheric circulation is reducing the lifetime of these GHGs. We aim to analyse these discrepancies in future studies. Finally, analysis of TCOM-CH<sub>4</sub> and TOMCAT CH<sub>4</sub> profiles suggests that the representation of QBO-induced secondary circulation is not adequate in the CTM and differences also reveal some temporal inhomogeneities in ERA5 reanalysis data.

Presently, the TCOM-CH<sub>4</sub> and TCOM-N<sub>2</sub>O V1.0 data set is ideally suited for the evaluation of CH<sub>4</sub> and N<sub>2</sub>O chemistry and stratospheric transport processes in models. The TCOM-CH<sub>4</sub> data set can also be used as realistic stratospheric profiles in a CH<sub>4</sub> profile/total column retrievals. Daily mean zonal mean TCOM-CH<sub>4</sub> and TCOM-N<sub>2</sub>O profile data on pressure and altitude levels in mixing ratio units are publicly available via <https://doi.org/10.5281/zenodo.7293740> (Dhomse, 2022a) and <https://doi.org/10.5281/zenodo.7386001> (Dhomse, 2022b), respectively.

## 7 Data availability

HALOE V19 are from [https://acdisc.gesdisc.eosdis.nasa.gov/data//UARS\\_HALOE\\_Level2/](https://acdisc.gesdisc.eosdis.nasa.gov/data//UARS_HALOE_Level2/), ACE-FTS v4.2 is obtained via <http://www.ace.uwaterloo.ca/data.php>. SPARC climatological data can be obtained via doi:10.5281/zenodo.4265393 (Hegglin et al., 2021). TCOM-CH<sub>4</sub> and TCOM-N<sub>2</sub>O data are publicly available at <https://doi.org/10.5281/zenodo.7293740> (Dhomse, 2022a) and <https://doi.org/10.5281/zenodo.7386001> (Dhomse, 2022b), respectively.

*Author contributions.* SSD conceived and designed the study. MPC performed TOMCAT model simulations. SSD performed the analysis. SSD and MPC co-wrote the paper

*Competing interests.* Authors declare no conflicts of interests.

*Acknowledgements.* This work was supported by the NERC SISLAC (NE/R001782/1) and LSO3 (NE/V0011863/1) projects. We thank HALOE and ACE-FTS science teams for the data sets. We thank the European Centre for Medium-Range Weather Forecasts for providing their analyses. TOMCAT simulations were performed on the UK national Archer and Leeds Arc4 HPC systems.

425 **References**

- Arosio, C., Rozanov, A., Malinina, E., Eichmann, K.-U., von Clarmann, T., and Burrows, J. P.: Retrieval of ozone profiles from OMPS limb scattering observations, *Atmospheric Measurement Techniques*, 11, 2135–2149, <https://doi.org/10.5194/amt-11-2135-2018>, 2018.
- Baldwin, M. P., Gray, L. J., Dunkerton, T. J., Hamilton, K., Haynes, P. H., Randel, W. J., Holton, J. R., Alexander, M. J., Hirota, I., Horinouchi, T., Jones, D. B. A., Kinnersley, J. S., Marquardt, C., Sato, K., and Takahashi, M.: The quasi-biennial oscillation, *Reviews of Geophysics*, 39, 179–229, <https://doi.org/10.1029/1999RG000073>, 2001.
- 430 Bândă, N., Krol, M., van Weele, M., van Noije, T., and Röckmann, T.: Analysis of global methane changes after the 1991 Pinatubo volcanic eruption, *Atmospheric Chemistry and Physics*, 13, 2267–2281, <https://doi.org/10.5194/acp-13-2267-2013>, 2013.
- Bândă, N., Krol, M., van Weele, M., van Noije, T., Le Sager, P., and Röckmann, T.: Can we explain the observed methane variability after the Mount Pinatubo eruption?, *Atmospheric Chemistry and Physics*, 16, 195–214, <https://doi.org/10.5194/acp-16-195-2016>, 2016.
- 435 Bernath, P.: Atmospheric Chemistry Experiment (ACE): An overview, *IEEE International Geoscience and Remote Sensing Symposium*, 2, 147–160, <http://eprints.whiterose.ac.uk/68898/>, 2002.
- Bernath, P. F., McElroy, C. T., Abrams, M. C., Boone, C. D., Butler, M., Camy-Peyret, C., Carleer, M., Clerbaux, C., Coheur, P.-F., Colin, R., DeCola, P., DeMazière, M., Drummond, J. R., Dufour, D., Evans, W. F. J., Fast, H., Fussen, D., Gilbert, K., Jennings, D. E., Llewellyn, E. J., Lowe, R. P., Mahieu, E., McConnell, J. C., McHugh, M., McLeod, S. D., Michaud, R., Midwinter, C., Nassar, R., Nichitiu, F., 440 Nowlan, C., Rinsland, C. P., Rochon, Y. J., Rowlands, N., Semeniuk, K., Simon, P., Skelton, R., Sloan, J. J., Soucy, M.-A., Strong, K., Tremblay, P., Turnbull, D., Walker, K. A., Walkty, I., Wardle, D. A., Wehrle, V., Zander, R., and Zou, J.: Atmospheric Chemistry Experiment (ACE): Mission overview, *Geophysical Research Letters*, 32, <https://doi.org/https://doi.org/10.1029/2005GL022386>, 2005.
- Bittner, M., Schmidt, H., Timmreck, C., and Sienz, F.: Using a large ensemble of simulations to assess the Northern Hemisphere stratospheric dynamical response to tropical volcanic eruptions and its uncertainty, *Geophysical Research Letters*, 43, 9324–9332, 445 <https://doi.org/10.1002/2016GL070587>, 2016.
- Boone, C., Bernath, P., Cok, D., Jones, S., and Steffen, J.: Version 4 retrievals for the atmospheric chemistry experiment Fourier transform spectrometer (ACE-FTS) and imagers, *Journal of Quantitative Spectroscopy and Radiative Transfer*, 247, 106939, <https://doi.org/https://doi.org/10.1016/j.jqsrt.2020.106939>, 2020.
- Chen, T. and Guestrin, C.: Xgboost: A scalable tree boosting system, in: *Proceedings of the 22nd acm sigkdd international conference on knowledge discovery and data mining*, pp. 785–794, 2016.
- 450 Chipperfield, M., Liang, Q., Abraham, L., Bekki, S., Braesicke, P., Dhomse, S., Genova, G. D., Fleming, E., Hardiman, S. C., Iachettii, D., Jackman, C. H., Kinnison, D. E., Marchand, M., Pitari, G., Rozanov, E., Stenke, A., and Tummon, F.: Lifetimes of Stratospheric Ozone-Depleting Substances, Their Replacements, and Related Species, Tech. rep., SPARC, <http://www.sparc-climate.org/fileadmin/customer/6{ }Publications/SPARC{ }reports{ }PDF/6{ }LifetimeReport{ }Ch5.pdf><http://www.sparc-climate.org/publications/sparc-reports/sparc-report-no6/>, 2013.
- 455 Chipperfield, M. P.: New version of the TOMCAT/SLIMCAT off-line chemical transport model: Intercomparison of stratospheric tracer experiments, *Quarterly Journal of the Royal Meteorological Society*, 132, 1179–1203, <https://doi.org/10.1256/qj.05.51>, 2006.
- Davis, S. M., Rosenlof, K. H., Hassler, B., Hurst, D. F., Read, W. G., Vömel, H., Selkirk, H., Fujiwara, M., and Damadeo, R.: The Stratospheric Water and Ozone Satellite Homogenized (SWOOSH) database: a long-term database for climate studies, *Earth System Science Data*, 8, 461–490, <https://doi.org/10.5194/essd-8-461-2016>, 2016.
- 460

- Dhomse, S.: TCOM-CH4: TOMCAT CTM and Occultation Measurements based daily zonal stratospheric methane profile dataset [1991-2021] constructed using machine-learning, <https://doi.org/10.5281/zenodo.7293740>, 2022a.
- Dhomse, S.: TCOM-N2O: TOMCAT CTM and Occultation Measurements based daily zonal stratospheric nitrous oxide profile dataset [1991-2021] constructed using machine-learning, <https://doi.org/10.5281/zenodo.7386001>, 2022b.
- 465 Dhomse, S. S., Chipperfield, M. P., Feng, W., Hossaini, R., Mann, G. W., and Santee, M. L.: Revisiting the hemispheric asymmetry in midlatitude ozone changes following the Mount Pinatubo eruption: A 3-D model study, *Geophysical Research Letters*, 42, 3038–3047, <https://doi.org/10.1002/2015GL063052>, 2015.
- Dhomse, S. S., Chipperfield, M. P., Damadeo, R. P., Zawodny, J. M., Ball, W. T., Feng, W., Hossaini, R., Mann, G. W., and Haigh, J. D.: On the ambiguous nature of the 11-year solar cycle signal in upper stratospheric ozone, *Geophysical Research Letters*, 43, 7241–7249, <https://doi.org/10.1002/2016GL069958>, 2016.
- 470 Dhomse, S. S., Mann, G. W., Antuña Marrero, J. C., Shallcross, S. E., Chipperfield, M. P., Carslaw, K. S., Marshall, L., Abraham, N. L., and Johnson, C. E.: Evaluating the simulated radiative forcings, aerosol properties, and stratospheric warmings from the 1963 Mt Agung, 1982 El Chichón, and 1991 Mt Pinatubo volcanic aerosol clouds, *Atmospheric Chemistry and Physics*, 20, 13 627–13 654, <https://doi.org/10.5194/acp-20-13627-2020>, 2020.
- 475 Dhomse, S. S., Arosio, C., Feng, W., Rozanov, A., Weber, M., and Chipperfield, M. P.: ML-TOMCAT: machine-learning-based satellite-corrected global stratospheric ozone profile data set from a chemical transport model, *Earth System Science Data*, 13, 5711–5729, <https://doi.org/10.5194/essd-13-5711-2021>, 2021.
- Dhomse, S. S., Chipperfield, M. P., Feng, W., Hossaini, R., Mann, G. W., Santee, M. L., and Weber, M.: A single-peak-structured solar cycle signal in stratospheric ozone based on Microwave Limb Sounder observations and model simulations, *Atmospheric Chemistry and Physics*, 22, 903–916, 2022.
- 480 Diallo, M. A., Ploeger, F., Hegglin, M. I., Ern, M., Grooß, J.-U., Khaykin, S., and Riese, M.: Stratospheric water vapour and ozone response to the quasi-biennial oscillation disruptions in 2016 and 2020, *Atmospheric Chemistry and Physics*, 22, 14 303–14 321, <https://doi.org/10.5194/acp-22-14303-2022>, 2022.
- Drummond, J., Houghton, J. T., Peskett, G., Rodgers, C., Wale, M., Whitney, J., and Williamson, E.: The stratospheric and mesospheric sounder on Nimbus 7, *Philosophical Transactions of the Royal Society of London. Series A, Mathematical and Physical Sciences*, 296, 219–241, 1980.
- 485 Farman, J. C., Gardiner, B. G., and Shanklin, J. D.: Large losses of total ozone in Antarctica reveal seasonal ClO x/NO x interaction, *Nature*, 315, 207–210, 1985.
- Free, M. and Lanzante, J.: Effect of Volcanic Eruptions on the Vertical Temperature Profile in Radiosonde Data and Climate Models, *Journal of Climate*, 22, 2925–2939, <https://doi.org/10.1175/2008JCLI2562.1>, 2009.
- 490 Gunson, M., Farmer, C. B., Norton, R., Zander, R., Rinsland, C. P., Shaw, J., and Gao, B.-C.: Measurements of CH<sub>4</sub>, N<sub>2</sub>O, CO, H<sub>2</sub>O, and O<sub>3</sub> in the middle atmosphere by the Atmospheric Trace Molecule Spectroscopy Experiment on Spacelab 3, *Journal of Geophysical Research: Atmospheres*, 95, 13 867–13 882, 1990.
- Hassler, B., Bodeker, G., and Dameris, M.: A new global database of trace gases and aerosols from multiple sources of high vertical resolution measurements, *Atmospheric Chemistry and Physics*, 8, 5403–5421, 2008.
- 495 Hassler, B., Kremser, S., Bodeker, G. E., Lewis, J., Nesbit, K., Davis, S. M., Chipperfield, M. P., Dhomse, S. S., and Dameris, M.: An updated version of a gap-free monthly mean zonal mean ozone database, *Earth System Science Data*, 10, 1473–1490, 2018.

- Hegglin, M. I., Tegtmeier, S., Anderson, J., Bourassa, A. E., Brohede, S., Degenstein, D., Froidevaux, L., Funke, B., Gille, J., Kasai, Y., Kyrölä, E., Lumpe, J., Murtagh, D., Neu, J. L., Pérot, K., Remsberg, E., Rozanov, A., Toohey, M., von Clarmann, T., Walker, K. A., Wang, H. J., Damadeo, R., Fuller, R., Lingenfelter, G., Roth, C., Ryan, N. J., Sioris, C., Smith, L., and Weigel, K.: SPARC Data Initiative monthly zonal mean composition measurements from stratospheric limb sounders (1978–2018), <https://doi.org/10.5281/zenodo.4265393>, 2020.
- Hegglin, M. I., Tegtmeier, S., Anderson, J., Bourassa, A. E., Brohede, S., Degenstein, D., Froidevaux, L., Funke, B., Gille, J., Kasai, Y., Kyrölä, E. T., Lumpe, J., Murtagh, D., Neu, J. L., Pérot, K., Remsberg, E. E., Rozanov, A., Toohey, M., Urban, J., von Clarmann, T., Walker, K. A., Wang, H.-J., Arosio, C., Damadeo, R., Fuller, R. A., Lingenfelter, G., McLinden, C., Pendlebury, D., Roth, C., Ryan, N. J., Sioris, C., Smith, L., and Weigel, K.: Overview and update of the SPARC Data Initiative: comparison of stratospheric composition measurements from satellite limb sounders, *Earth System Science Data*, 13, 1855–1903, <https://doi.org/10.5194/essd-13-1855-2021>, 2021.
- Hersbach, H., Bell, B., Berrisford, P., Hirahara, S., Horányi, A., Muñoz-Sabater, J., Nicolas, J., Peubey, C., Radu, R., Schepers, D., Simmons, A., Soci, C., Abdalla, S., Abellan, X., Balsamo, G., Bechtold, P., Biavati, G., Bidlot, J., Bonavita, M., De Chiara, G., Dahlgren, P., Dee, D., Diamantakis, M., Dragani, R., Flemming, J., Forbes, R., Fuentes, M., Geer, A., Haimberger, L., Healy, S., Hogan, R. J., Hólm, E., Janisková, M., Keeley, S., Laloyaux, P., Lopez, P., Lupu, C., Radnoti, G., de Rosnay, P., Rozum, I., Vamborg, F., Villaume, S., and Thépaut, J.-N.: The ERA5 global reanalysis, *Quarterly Journal of the Royal Meteorological Society*, 146, 1999–2049, <https://doi.org/https://doi.org/10.1002/qj.3803>, 2020.
- Inness, A., Blechschmidt, A.-M., Bouarar, I., Chabrilat, S., Crepulja, M., Engelen, R. J., Eskes, H., Flemming, J., Gaudel, A., Hendrick, F., Huijnen, V., Jones, L., Kapsomenakis, J., Katragkou, E., Keppens, A., Langerock, B., de Mazière, M., Melas, D., Parrington, M., Peuch, V. H., Razinger, M., Richter, A., Schultz, M. G., Suttie, M., Thouret, V., Vrekoussis, M., Wagner, A., and Zerefos, C.: Data assimilation of satellite-retrieved ozone, carbon monoxide and nitrogen dioxide with ECMWF’s Composition-IFS, *Atmospheric Chemistry and Physics*, 15, 5275–5303, <https://doi.org/10.5194/acp-15-5275-2015>, 2015.
- Jones, R. and Pyle, J.: Observations of CH<sub>4</sub> and N<sub>2</sub>O by the Nimbus 7 SAMS: A comparison with in situ data and two-dimensional numerical model calculations, *Journal of Geophysical Research: Atmospheres*, 89, 5263–5279, 1984.
- Lan, X., Nisbet, E. G., Dlugokencky, E. J., and Michel, S. E.: What do we know about the global methane budget? Results from four decades of atmospheric CH<sub>4</sub> observations and the way forward, *Philosophical Transactions of the Royal Society A: Mathematical, Physical and Engineering Sciences*, 379, 20200440, <https://doi.org/10.1098/rsta.2020.0440>, 2021.
- Lelieveld, J., Crutzen, P. J., and Dentener, F. J.: Changing concentration, lifetime and climate forcing of atmospheric methane, *Tellus B*, 50, 128–150, 1998.
- Li, Y., Dhomse, S. S., Chipperfield, M. P., Feng, W., Chrysanthou, A., Xia, Y., and Guo, D.: Effects of reanalysis forcing fields on ozone trends and age of air from a chemical transport model, *Atmospheric Chemistry and Physics*, 22, 10635–10656, <https://doi.org/10.5194/acp-22-10635-2022>, 2022.
- Livesey, N. J., Read, W. G., Froidevaux, L., Lambert, A., Santee, M. L., Schwartz, M. J., Millán, L. F., Jarnot, R. F., Wagner, P. A., Hurst, D. F., Walker, K. A., Sheese, P. E., and Nedoluha, G. E.: Investigation and amelioration of long-term instrumental drifts in water vapor and nitrous oxide measurements from the Aura Microwave Limb Sounder (MLS) and their implications for studies of variability and trends, *Atmospheric Chemistry and Physics*, 21, 15409–15430, <https://doi.org/10.5194/acp-21-15409-2021>, 2021.
- Meinshausen, M., Nicholls, Z. R. J., Lewis, J., Gidden, M. J., Vogel, E., Freund, M., Beyerle, U., Gessner, C., Nauels, A., Bauer, N., Canadell, J. G., Daniel, J. S., John, A., Krummel, P. B., Luderer, G., Meinshausen, N., Montzka, S. A., Rayner, P. J., Reimann, S., Smith, S. J., van den

- 535 Berg, M., Velders, G. J. M., Vollmer, M. K., and Wang, R. H. J.: The shared socio-economic pathway (SSP) greenhouse gas concentrations and their extensions to 2500, *Geoscientific Model Development*, 13, 3571–3605, <https://doi.org/10.5194/gmd-13-3571-2020>, 2020.
- Minganti, D., Chabrillat, S., Errera, Q., Prignon, M., Kinnison, D. E., Garcia, R. R., Abalos, M., Alsing, J., Schneider, M., Smale, D., Jones, N., and Mahieu, E.: Evaluation of the N<sub>2</sub>O Rate of Change to Understand the Stratospheric Brewer-Dobson Circulation in a Chemistry-Climate Model, *Journal of Geophysical Research: Atmospheres*, 127, e2021JD036390, <https://doi.org/https://doi.org/10.1029/2021JD036390>, e2021JD036390 2021JD036390, 2022.
- 540 Newman, P., Coy, L., Pawson, S., and Lait, L.: The anomalous change in the QBO in 2015–2016, *Geophysical Research Letters*, 43, 8791–8797, 2016.
- Nisbet, E. G., Manning, M., Dlugokencky, E., Fisher, R., Lowry, D., Michel, S., Myhre, C. L., Platt, S. M., Allen, G., Bousquet, P., et al.: Very strong atmospheric methane growth in the 4 years 2014–2017: Implications for the Paris Agreement, *Global Biogeochemical Cycles*, 33, 318–342, 2019.
- 545 Noël, S., Bramstedt, K., Hilker, M., Liebing, P., Plieninger, J., Reuter, M., Rozanov, A., Sioris, C. E., Bovensmann, H., and Burrows, J. P.: Stratospheric CH<sub>4</sub> and CO<sub>2</sub> profiles derived from SCIAMACHY solar occultation measurements, *Atmospheric Measurement Techniques*, 9, 1485–1503, 2016.
- Noël, S., Weigel, K., Bramstedt, K., Rozanov, A., Weber, M., Bovensmann, H., and Burrows, J. P.: Water vapour and methane coupling in the stratosphere observed using SCIAMACHY solar occultation measurements, *Atmospheric Chemistry and Physics*, 18, 4463–4476, 2018.
- 550 Osprey, S. M., Butchart, N., Knight, J. R., Scaife, A. A., Hamilton, K., Anstey, J. A., Schenzinger, V., and Zhang, C.: An unexpected disruption of the atmospheric quasi-biennial oscillation, *Science*, <https://doi.org/10.1126/science.aah4156>, 2016.
- Poberaj, C. S., Staehelin, J., and Brunner, D.: Missing Stratospheric Ozone Decrease at Southern Hemisphere Middle Latitudes after Mt. Pinatubo: A Dynamical Perspective, *Journal of the Atmospheric Sciences*, 68, 1922–1945, <https://doi.org/10.1175/JAS-D-10-05004.1>, 2011.
- 555 Prather, M. J., Froidevaux, L., and Livesey, N. J.: Observed changes in stratospheric circulation: Decreasing lifetime of N<sub>2</sub>O, 2005–2021, *Atmospheric Chemistry and Physics Discussions*, 2022, 1–13, <https://doi.org/10.5194/acp-2022-650>, 2022.
- Randel, W. J. and Wu, F.: A stratospheric ozone profile data set for 1979–2005: Variability, trends, and comparisons with column ozone data, *Journal of Geophysical Research: Atmospheres*, 112, 2007.
- 560 Remedios, J., Ruth, S., Rodgers, C., Taylor, F., Roche, A., Gille, J., Gunson, M., Russell III, J., Park, J., and Zipf, E.: Measurements of methane and nitrous oxide distributions by the improved stratospheric and mesospheric sounder: Retrieval and validation, *Journal of Geophysical Research: Atmospheres*, 101, 9843–9871, 1996.
- Remsberg, E.: On the response of Halogen Occultation Experiment (HALOE) stratospheric ozone and temperature to the 11-year solar cycle forcing, *Journal of Geophysical Research: Atmospheres* . . . , <http://onlinelibrary.wiley.com/doi/10.1029/2008JD010189/full>, 2008.
- 565 Remsberg, E. E.: Methane as a diagnostic tracer of changes in the Brewer–Dobson circulation of the stratosphere, *Atmospheric Chemistry and Physics*, 15, 3739–3754, <https://doi.org/10.5194/acp-15-3739-2015>, 2015.
- Russell III, J. M., Gordley, L. L., Park, J. H., Drayson, S. R., Hesketh, W. D., Cicerone, R. J., Tuck, A. F., Frederick, J. E., Harries, J. E., and Crutzen, P. J.: The halogen occultation experiment, *Journal of Geophysical Research: Atmospheres*, 98, 10 777–10 797, 1993.
- Saunois, M., Bousquet, P., Poulter, B., Peregón, A., Ciais, P., Canadell, J. G., Dlugokencky, E. J., Etiope, G., Bastviken, D., Houweling, S., et al.: The global methane budget 2000–2012, *Earth System Science Data*, 8, 697–751, 2016.
- 570 Strong, K., Wolff, M. A., Kerzenmacher, T. E., Walker, K. A., Bernath, P. F., Blumenstock, T., Boone, C., Catoire, V., Coffey, M., De Mazière, M., Demoulin, P., Duchatelet, P., Dupuy, E., Hannigan, J., Höpfner, M., Glatthor, N., Griffith, D. W. T., Jin, J. J., Jones, N., Jucks, K.,

- Kuellmann, H., Kuttippurath, J., Lambert, A., Mahieu, E., McConnell, J. C., Mellqvist, J., Mikuteit, S., Murtagh, D. P., Notholt, J., Piccolo, C., Raspollini, P., Ridolfi, M., Robert, C., Schneider, M., Schrems, O., Semeniuk, K., Senten, C., Stiller, G. P., Strandberg, A., Taylor, J., Tétard, C., Toohey, M., Urban, J., Warneke, T., and Wood, S.: Validation of ACE-FTS N<sub>2</sub>O measurements, *Atmospheric Chemistry and Physics*, 8, 4759–4786, <https://doi.org/10.5194/acp-8-4759-2008>, 2008.
- 575 Tian, H., Xu, R., Canadell, J. G., Thompson, R. L., Winiwarter, W., Suntharalingam, P., Davidson, E. A., Ciais, P., Jackson, R. B., Janssens-Maenhout, G., Prather, M. J., Regnier, P., Pan, N., Pan, S., Peters, G. P., Shi, H., Tubiello, F. N., Zaehele, S., Zhou, F., Arneeth, A., Battaglia, G., Berthet, S., Bopp, L., Bouwman, A. F., Buitenhuis, E. T., Chang, J., Chipperfield, M. P., Dangal, S. R. S., Dlugokencky, E., Elkins, J. W., Eyre, B. D., Fu, B., Hall, B., Ito, A., Joos, F., Krummel, P. B., Landolfi, A., Laruelle, G. G., Lauerwald, R., Li, W., Lienert, S., Maavara, T., MacLeod, M., Millet, D. B., Olin, S., Patra, P. K., Prinn, R. G., Raymond, P. A., Ruiz, D. J., van der Werf, G. R., Vuichard, N., Wang, J., Weiss, R. F., Wells, K. C., Wilson, C., Yang, J., and Yao, Y.: A comprehensive quantification of global nitrous oxide sources and sinks, *Nature*, 586, 248–256, 2020.
- 580 Urban, J., Lautié, N., Le Flochmoën, E., Jiménez, C., Eriksson, P., de La Noë, J., Dupuy, E., El Amraoui, L., Frisk, U., Jégou, F., Murtagh, D., Olberg, M., Ricaud, P., Camy-Peyret, C., Dufour, G., Payan, S., Huret, N., Pirre, M., Robinson, A. D., Harris, N. R. P., Bremer, H., Kleinböhl, A., Küllmann, K., Künzi, K., Kuttippurath, J., Ejiri, M. K., Nakajima, H., Sasano, Y., Sugita, T., Yokota, T., Piccolo, C., Raspollini, P., and Ridolfi, M.: Odin/SMR limb observations of stratospheric trace gases: Validation of N<sub>2</sub>O, *Journal of Geophysical Research: Atmospheres*, 110, <https://doi.org/https://doi.org/10.1029/2004JD005394>, 2005.
- 590 Waters, J. W., Froidevaux, L., Harwood, R. S., Jarnot, R. F., Pickett, H. M., Read, W. G., Siegel, P. H., Cofield, R. E., Filipiak, M. J., Flower, D. A., et al.: The earth observing system microwave limb sounder (EOS MLS) on the Aura satellite, *IEEE transactions on geoscience and remote sensing*, 44, 1075–1092, 2006.
- WMO: Scientific Assessment of Ozone Depletion:2018, Tech. rep., World Meteorological Organization, Global Ozone Research and Monitoring Project, Report No. 58, Geneva, Switzerland, <https://www.wmo.int/pages/prog/arep/gaw/ozone{ }2018/>, 2018.

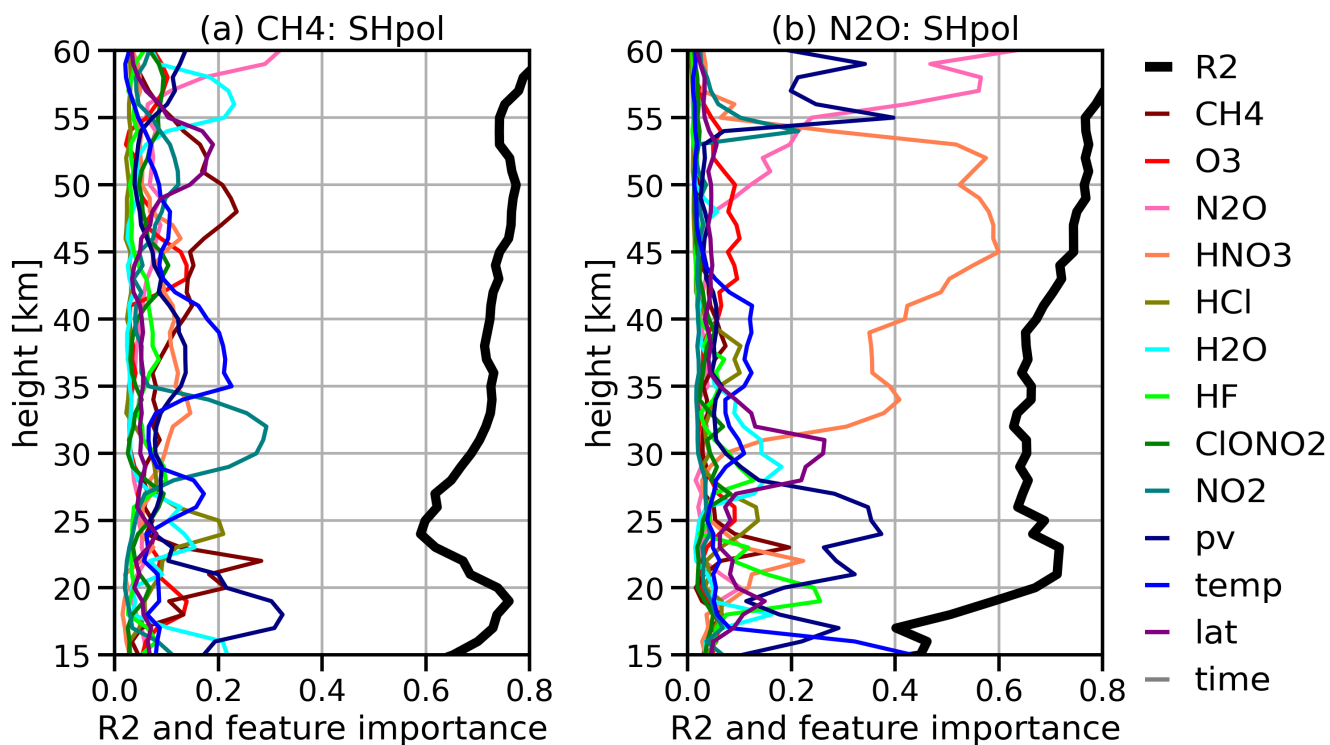


**Figure 1.** Vertical profiles of the variance ( $R^2$ ) and feature importances estimated by XGBoost regression models for the TOMCAT-observation differences for (a) CH<sub>4</sub> (1991-2018) and (b) N<sub>2</sub>O (2004-2018, ACE only) for the SHpol (50°S–90°S) latitude bin. See equation 1 and subsequent information about the features (total 13) for variables used in the XGBoost regression model.



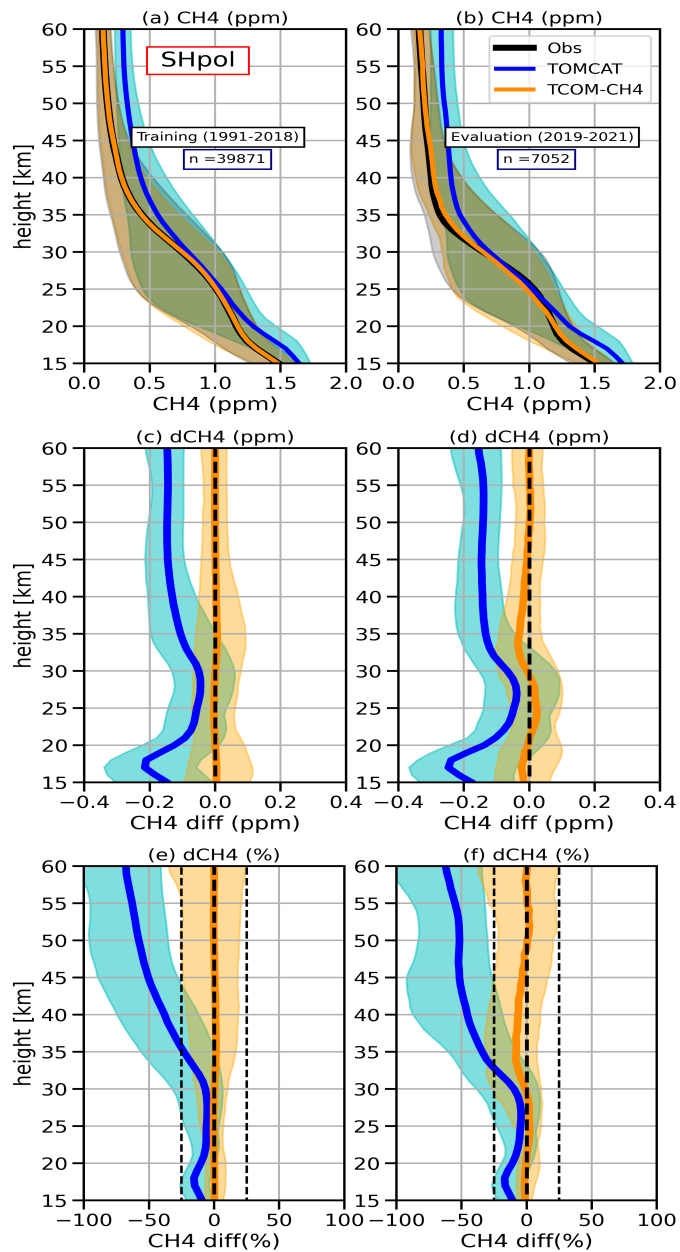


**Figure 2.** Panels (a) and (b). Comparison between TOMCAT (blue), TCOM-CH4 (orange) and satellite measurement-based (black) CH<sub>4</sub> profiles for the SHpol (50°S–90°S) latitude band. Solid lines indicate median profiles while shaded regions show 10th and 90th percentile range. Comparisons are shown for training (1992–2018) and evaluation (2019–2021) periods in panels (a, left) and (b, right), respectively. Panels (c) - (f) show differences between TOMCAT and TCOM-CH4 w. r. t. satellite data sets in absolute units (ppm) and percent. Right (c and e) and left (d and f) panels show differences for the training (1992–2018) and evaluation (2019–2021) periods.

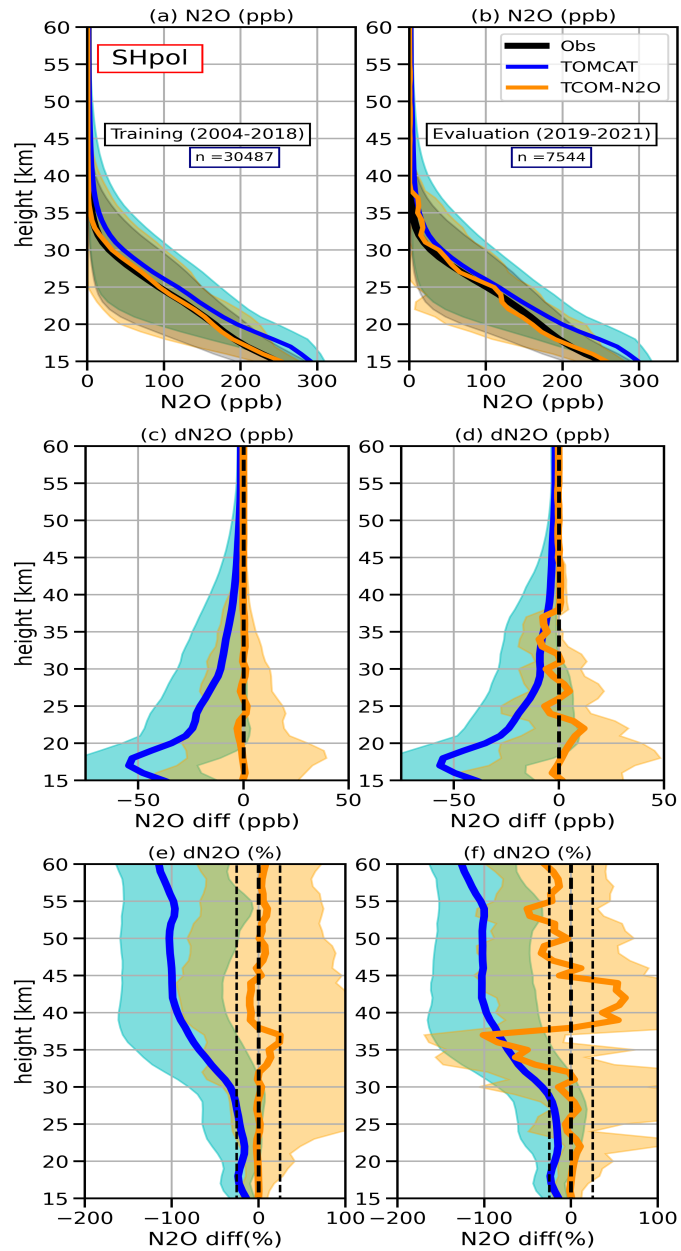


**Figure 3.** Same as Figure 2, but for N<sub>2</sub>O. The training period includes data for 2004–2018.

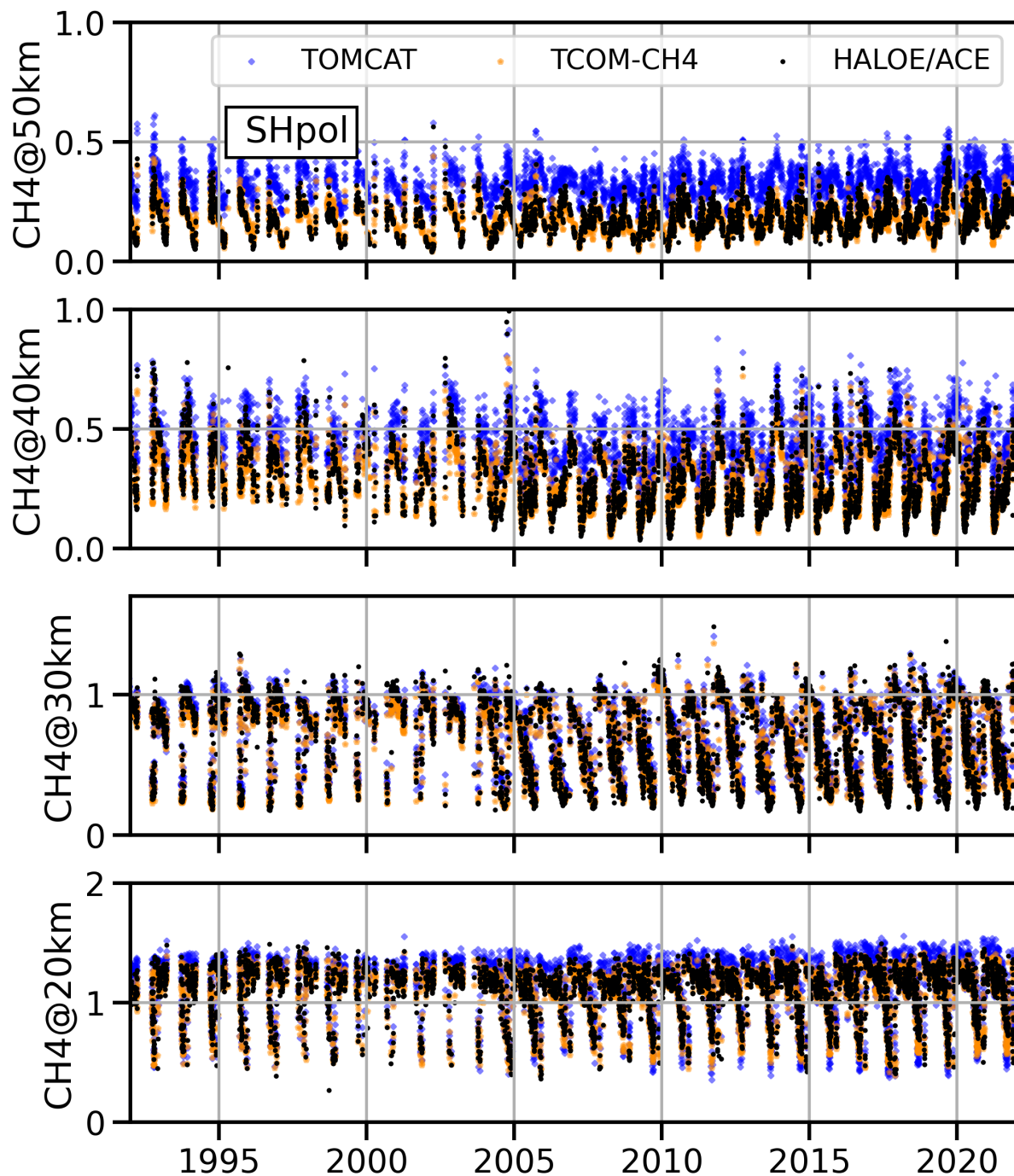


**Figure 4.** Time evolution (1992-2021) of CH<sub>4</sub> (in ppm) from TOMCAT (blue crosses), TCOM-CH4 (orange diamonds) and satellite data (black dots) for SHpol (50°S–90°S) at 20, 30, 40 and 50 km. Note that for clarity only 10% (every 10th) of data points are shown. Due to the sharp gradient in the vertical distribution, the y axis range varies between the panels.

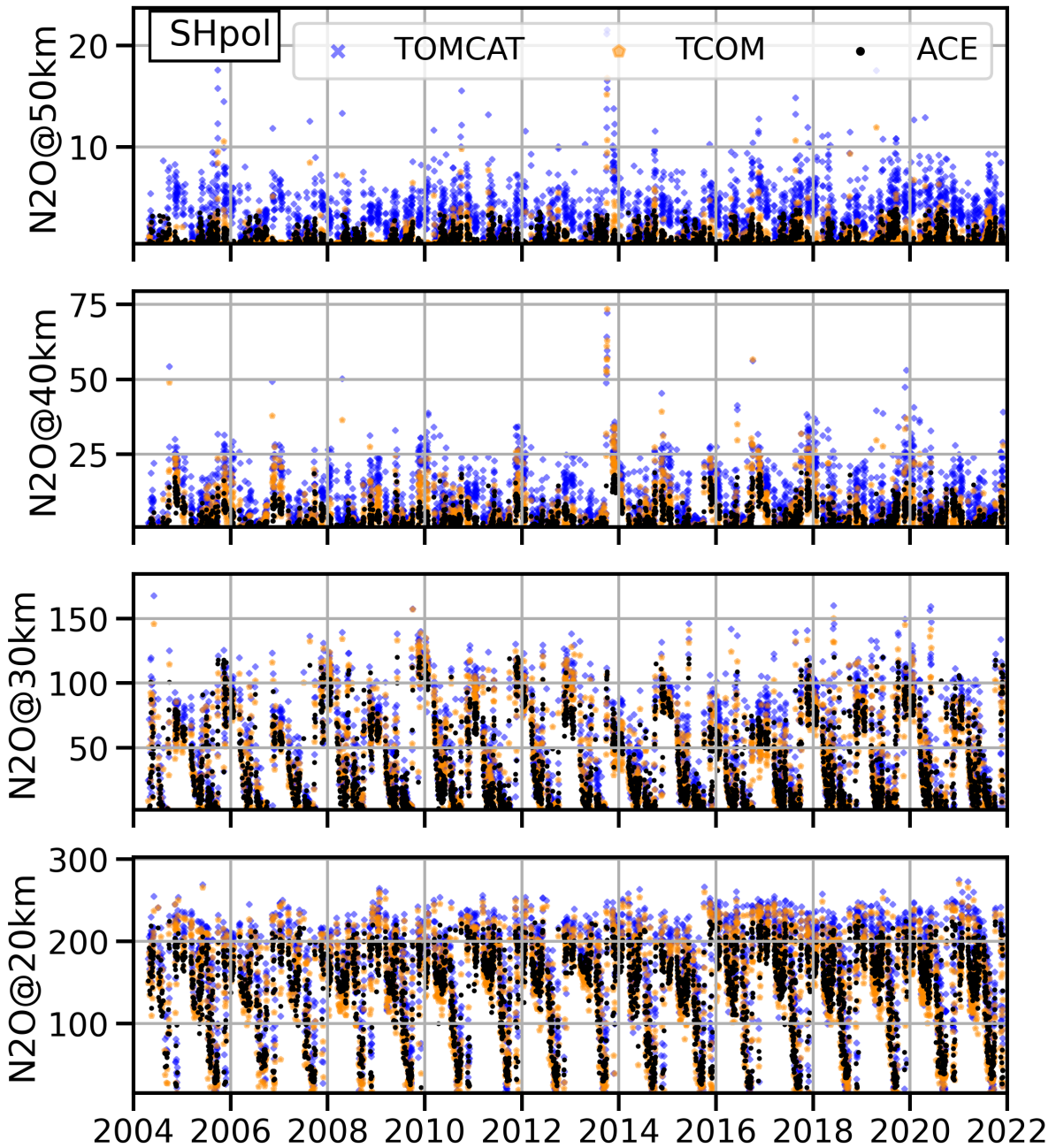


**Figure 5.** Same as Figure 4, but for N<sub>2</sub>O (in ppb). The comparison is shown for the 2004-2021 time period.

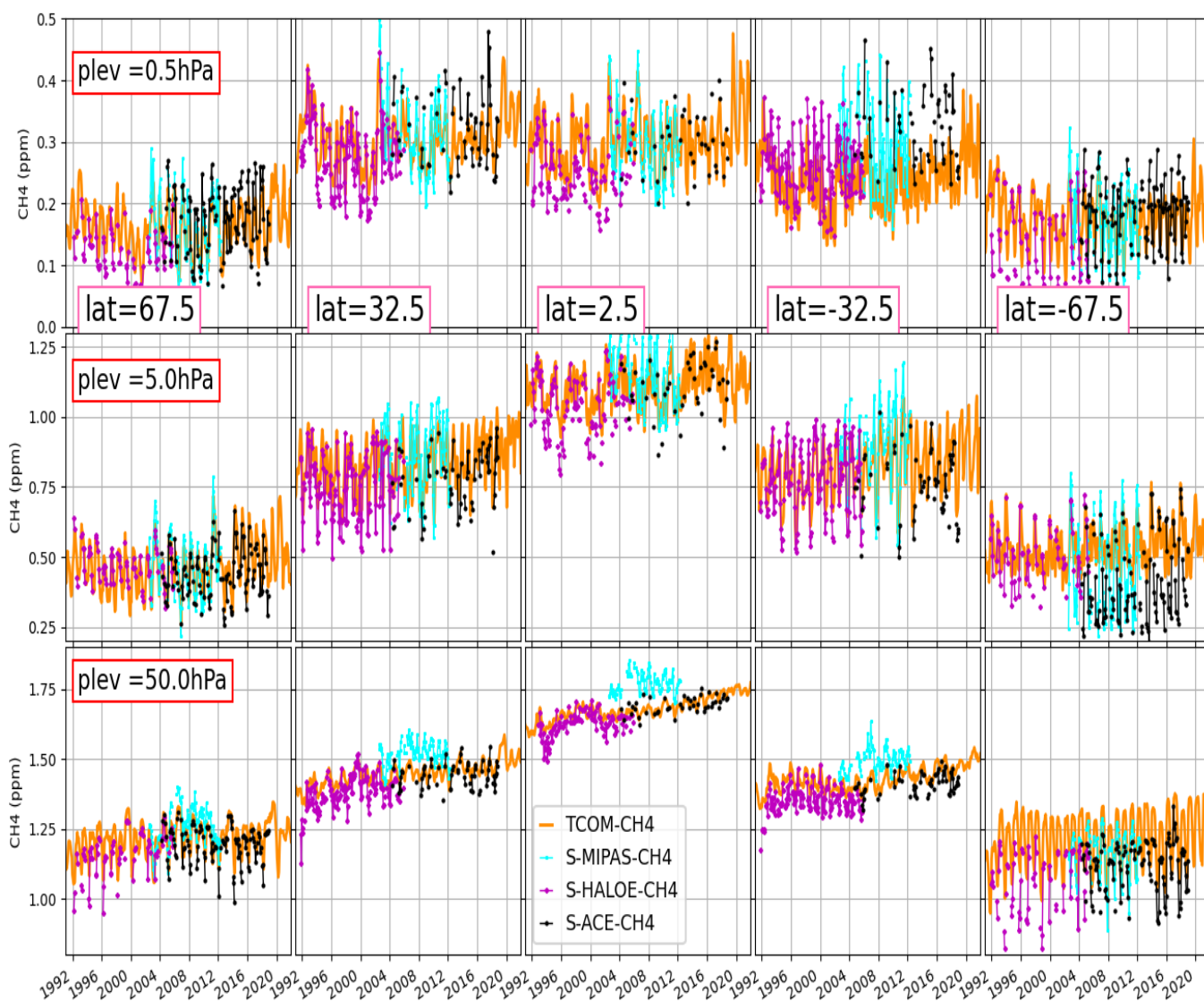


**Figure 6.** Comparison between TCOM-CH4 (dark line) and three (ACE (black line), HALOE (magenta line) and MIPAS (aqua line)) satellite instrument-based SPARC-CH4 data sets (for details see Hegglin et al. (2021)). Time series of monthly mean values from SPARC-CH4 and TCOM-CH4 data set are shown for 0.5 hPa (top), 5 hPa (middle), and 50 hPa (bottom) for five latitude bins: 67.5° and 32.5° in both hemispheres as well as 2.5°N (middle).





**Figure 7.** Same as Figure 6 but for  $\text{N}_2\text{O}$ . SPARC data from the four satellite instruments ACE (v3.6), Aura-MLS (v4), MIPAS (v422) and SMR (v2.1) are shown with black, green, aqua and pink coloured lines, respectively.

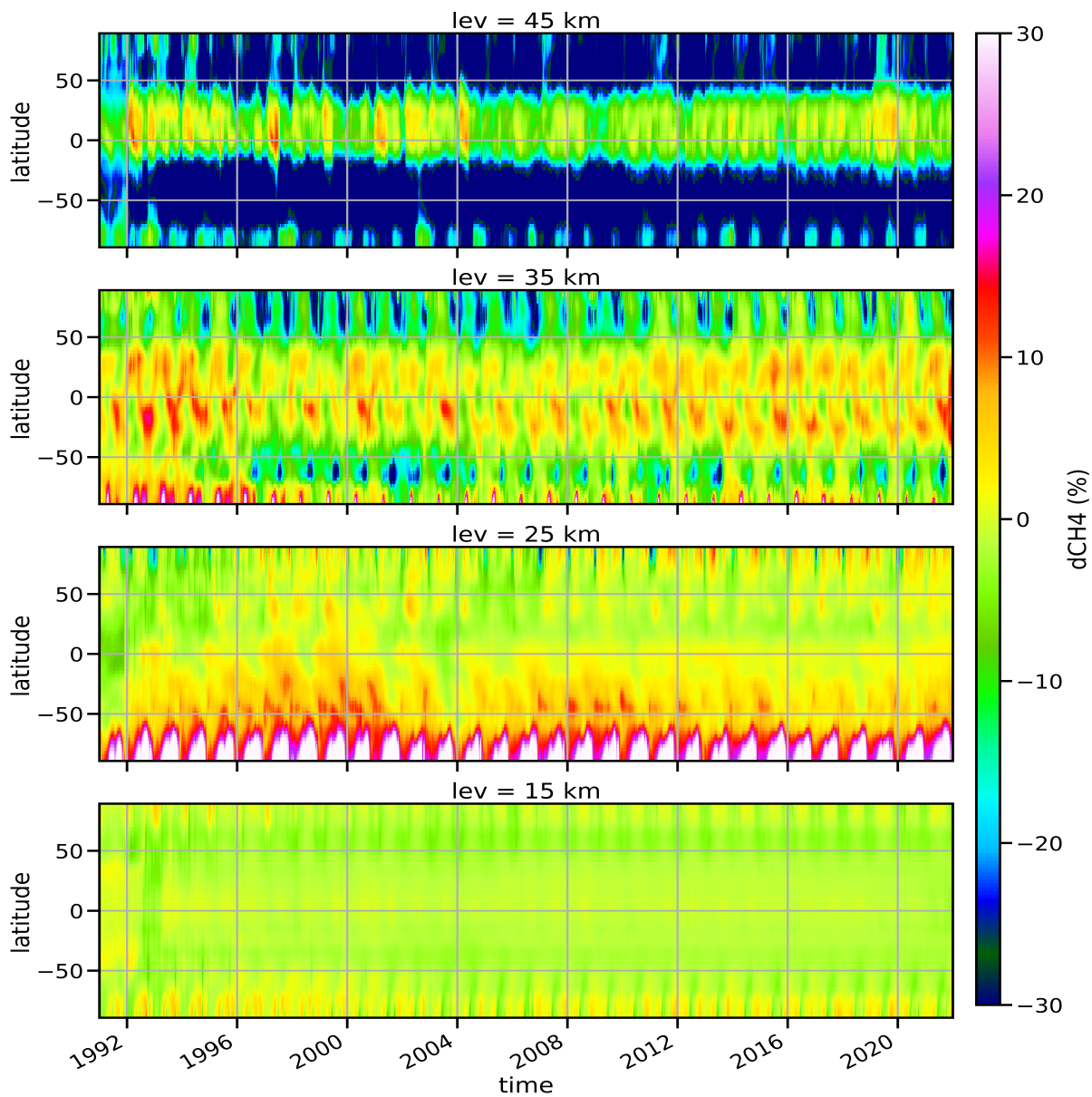


**Figure 8.** Latitude-time cross section of the differences between TCOM-CH<sub>4</sub> and TOMCAT CTM CH<sub>4</sub> profiles (in %) at 15 km (bottom), 25 km, 35 km and 45 km (top). Percent differences are calculated as  $200 \times (\text{TCOM}-\text{TOMCAT})/(\text{TCOM}+\text{TOMCAT})$ .